Article

Electron Transfer at a Dithiolate-Bridged Diiron Assembly: Electrocatalytic Hydrogen Evolution

Stacey J. Borg, Thomas Behrsing, Stephen P. Best, Mathieu Razavet, Xiaoming Liu, and Christopher J. Pickett

J. Am. Chem. Soc., **2004**, 126 (51), 16988-16999• DOI: 10.1021/ja045281f • Publication Date (Web): 03 December 2004

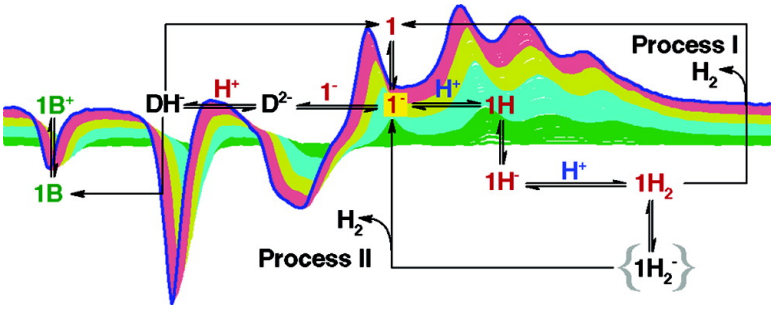

More About This Article

Additional resources and features associated with this article are available within the HTML version:

- Supporting Information
- Links to the 22 articles that cite this article, as of the time of this article download
- Access to high resolution figures
- Links to articles and content related to this article
- Copyright permission to reproduce figures and/or text from this article

View the Full Text HTML

J|A|C|S
ARTICLES
Published on Web 12/03/2004

Electron Transfer at a Dithiolate-Bridged Diiron Assembly: Electrocatalytic Hydrogen Evolution

Stacey J. Borg,[†] Thomas Behrsing,[†] Stephen P. Best,*[,†] Mathieu Razavet,[‡] Xiaoming Liu,[‡] and Christopher J. Pickett*[,‡]

Contribution from the School of Chemistry, University of Melbourne 3010, Victoria, Australia, and Department of Biological Chemistry, The John Innes Centre, Research Park, Colney, Norwich NR4 7UH, U.K.

Received August 5, 2004; E-mail: spbest@unimelb.edu.au (S.P.B.); chris.pickett@bbsrc.ac.uk (C.J.P.)

Abstract: Electrochemical reduction of $Fe_2(\mu\text{-pdt})(CO)_6$ **1** (pdt = propane-1,3-dithiolate) leads initially to a short-lived species, $\mathbf{1}^-$, then subsequently to two-electron reduced products, including a CO-bridged diiron compound, **1B**. The assignment of the redox level of $\mathbf{1}^-$ is based on EPR and UV−vis spectra together with the observation that a CO-saturated solution of $\mathbf{1}^-$ decays to give **1** and **1B**. Hydride reduction of **1** also results in formation of **1B** via a relatively long-lived formyl species, $\mathbf{1}_{\mathbf{formyl}}$. Despite its involvement in hydride transfer reactions, **1B** is formulated as $[Fe_2(\mu\text{-}S(CH_2)_3SH)(\mu\text{-}CO)(CO)_6]^-$ based on a range of spectroscopic measurements together with the Fe−Fe separation of 2.527 Å (EXAFS). Electrocatalytic proton reduction in the presence of **1** in moderately strong acids has been examined by electrochemical and spectroelectrochemical techniques. The acid concentration dependence of the voltammetry is modeled by a mechanism with two electron/proton additions leading to $\mathbf{1H_2}$, where dissociation of dihydrogen leads to recovery of **1**. Further reduction processes are evident at higher acid concentrations. Whereas free CO improves the reversibility of the electrochemistry of **1**, CO inhibits electrocatalytic proton reduction, and this occurs through side reactions involving a dimeric species formed from $\mathbf{1}^-$.

Introduction

The structure and function of the metal complexes at the active sites of the all-iron and nickel−iron hydrogenases[1,2] are receiving much attention because an understanding of the chemistry of their metallosulfur centers should lead to the design of artificial assemblies that provide inexpensive electrocatalytic materials. Catalysis of proton reduction by the all-iron hydrogenases occurs at rates in the order of 10^4 turnovers/s.[3] The center at which this fast chemistry takes place, the H-cluster, is comprised of a diiron subsite linked to a {4Fe4S}-cubane by a cysteinyl bridge.[2,4−6] The diiron subsite is extraordinary in that both cyanide and carbon monoxide are essential structural elements and that subvalent Fe^I redox states are involved in the catalytic cycle. That such a biologically unprecedented oxidation state is involved is powerfully supported by concordant chemical modeling,[7] theoretical calculations,[8,9] and $^{13}CO/^{12}CO$ FTIR studies[2,6] on the enzyme. Furthermore, in the paramagnetic resting state of the enzyme, a carbon monoxide ligand bridges the $\{Fe^I-Fe^{II}\}$ metal atoms,[5] a structural feature with biological precedence hitherto confined to a CO-inhibited state of the iron−molybdenum cofactor of nitrogenase.[10]

Biomimetic electrocatalytic proton reduction has been reported for dithiolate and bisthiolate-bridged diiron hexacarbonyl compounds,[11] as well as for their phosphine/cyano-substituted[12,13] or azadithiolate-bridged analogues.[14,15] The proposed reaction pathways involve protonation of the diiron bond, and depending on the σ-donor properties of the ligands, this may

[†] University of Melbourne.
[‡] The John Innes Centre.

(1) (a) Evans, D. J.; Pickett, C. J. *Chem. Soc. Rev.* **2003**, *32*, 268−275. (b) Cammack, R. *Nature* **1999**, *397*, 214−215. (c) Adams, M. W. W.; Stiefel, E. I. *Curr. Opin. Chem. Biol.* **2000**, *4*, 214−220. (d) Darensbourg, M. Y.; Lyon, E. J.; Smee, J. J. *Coord. Chem. Rev.* **2000**, *206*−*207*, 533−561. (e) Nicolet, Y.; Cavazza, C.; Fontecilla-Camps, J. C. *J. Inorg. Biochem.* **2002**, *91*, 1−8. (f) Georgakaki, I. P.; Darensbourg, M. Y. In *Comprehensive Coordination Chemistry II*; McCleverty, J. A., Meyer, T. J., Eds.; Elsevier: New York, 2004; Vol. 8, pp 549−568.
(2) Nicolet, Y.; de Lacey, A. L.; Vernède, X.; Fernandez, V. M.; Hatchikian, E. C.; Fontecilla-Camps, J. C. *J. Am. Chem. Soc.* **2001**, *123*, 1596−1601.
(3) Adams, M. W. W. *Biochim. Biophys. Acta* **1990**, *1020*, 115−145.
(4) (a) Nicolet, Y.; Piras, C.; Legrand, P.; Hatchikian, C. E.; Fontecilla-Camps, J. C. *Structure* **1999**, *7*, 13−23. (b) Lemon, B. J.; Peters, J. W. *Biochemistry* **1999**, *38*, 12969−12973. (c) Lemon, B. J.; Peters, J. W. *J. Am. Chem. Soc.* **2000**, *122*, 3793−3794. (d) Bennett, B.; Lemon, B. J.; Peters, J. W. *Biochemistry* **2000**, *39*, 7455−7460.
(5) Peters, J. W.; Lanzilotta, W. N.; Lemon, B. J.; Seefeldt, L. C. *Science* **1998**, *282*, 1853−1858 (Errata *283*, 35; *283*, 2102).
(6) De Lacey, A. L.; Stadler, C.; Cavazza, C.; Hatchikian, E. C.; Fernandez, V. M. *J. Am. Chem. Soc.* **2000**, *122*, 11232−11233.
(7) Razavet, M.; Borg, S. J.; George, S. J.; Best, S. P.; Fairhurst, S. A.; Pickett, C. J. *Chem. Commun.* **2002**, 700−701.
(8) (a) Dance, I. *Chem. Commun.* **1999**, 1655−1656. (b) Fan, H.-J.; Hall, M. B. *J. Am. Chem. Soc.* **2001**, *123*, 3828−3829. (c) Bruschi, M.; Fantucci, P.; De Gioia, L. *Inorg. Chem.* **2003**, *42*, 4773−4781. (d) Liu, Z.-P.; Hu, P. *J. Chem. Phys.* **2002**, *117*, 8177−8180.
(9) (a) Cao, Z.; Hall, M. B. *J. Am. Chem. Soc.* **2001**, *123*, 3734−3742. (b) Bruschi, M.; Fantucci, P.; De Gioia, L. *Inorg. Chem.* **2002**, *41*, 1421−1429. (c) Liu, Z.-P.; Hu, P. *J. Am. Chem. Soc.* **2002**, *124*, 5175−5182.
(10) (a) Pickett, C. J.; Vincent, K. A.; Ibrahim, S. K.; Gormal, C. A.; Smith, B. E.; Best, S. P. *Chem.—Eur. J.* **2003**, *9*, 76−87. (b) Lee, H.-I.; Cameron, L. M.; Hales, B. J.; Hoffman, B. M. *J. Am. Chem. Soc.* **1997**, *119*, 10121−10126.
(11) Chong, D.; Georgakaki, I. P.; Mejia-Rodriguez, R.; Sanabria-Chinchilla, J.; Soriaga, M. P.; Darensbourg, M. Y. *Dalton Trans.* **2003**, 4158−4163.
(12) Gloaguen, F.; Lawrence, J. D.; Rauchfuss, T. B.; Bénard, M.; Rohmer, M.-M. *Inorg. Chem.* **2002**, *41*, 6573−6582.
(13) Gloaguen, F.; Lawrence, J. D.; Rauchfuss, T. B. *J. Am. Chem. Soc.* **2001**, *123*, 9476−9477.
(14) Ott, S.; Kritikos, M.; Åkermark, B.; Sun, L.; Lomoth, R. *Angew Chem., Int. Ed.* **2004**, *43*, 1006−1009.

10.1021/ja045281f CCC: $27.50

occur either before or after one-electron reduction. Whereas the bridging metal hydrides have been characterized crystallographically[12,16] and protonation of the cyano ligands confirmed by IR spectroscopy,[12] the mechanism of the electrocatalytic reaction has not been subjected to quantitative analysis. For $Fe_2(\mu\text{-}PPh_2)_2(CO)_6$, the chemistry is dominated by two-electron reduction where both the singly and doubly protonated forms of the dianion give terminally bound iron hydrides,[17,18] and electrocatalytic proton reduction by the phosphido-bridged compounds in THF proceeds only after further reduction.[17] It is interesting that this electrochemical response is similar to that of $Fe_2(\mu\text{-}SEt)_2(CO)_6$ in the presence of acetic acid.[11] From the theoretical investigations of the mechanism of action of the H-cluster, there is no clear consensus as to whether terminally bound or bridging hydrides are more likely to be involved.[9,19] The previous experimental studies show that electrocatalytic proton reduction from diiron compounds with either terminal or bridging hydride ligands is feasible.

In this paper, we examine the products formed following reduction of the parent propanedithiolate-bridged diiron hexacarbonyl complex both in the presence and in the absence of protons. The form of the products obtained in these reactions will provide a basis for discussions of the mechanism of the electrochemical proton reductions catalyzed by dithiolate-bridged diiron compounds.

Results and Discussion

Electrochemistry of $Fe_2(\mu\text{-pdt})(CO)_6$, 1, (pdt = propane-1,3-dithiolate). The thiolate-bridged diiron hexacarbonyl compounds, $Fe_2(\mu\text{-}SR)_2(CO)_6$, have been reported to undergo a single chemically reversible two-electron reduction at moderately negative potentials (ca. −1.2 V).[20,21] [*All potentials in this paper are referenced to SCE.*] The chemical reversibility of the system (I_{pa}/I_{pc}) has been found to depend on the identity of the bridging ligands and is improved significantly by saturating the solution with CO.[21] Reduction of carefully dried acetonitrile solutions of **1** is almost reversible at low temperatures (−45 °C) or at room temperature for solutions saturated with CO (Supporting Information). The earlier two-electron assignment[21] of the process is at odds with a more recent study.[11] Moreover, equimolar mixtures of **1** and ferrocene (Fc) give similar values of ΔE_p and I_{pc} for the reduction of **1** and the Fc^+/Fc couple. At slower scan rates, the peak current function, $I_{pc}/\nu^{1/2}$, increases toward that expected for a two-electron process, and this is associated with the growth of additional daughter products evident in the anodic scan of the voltammogram. Addition of water to acetonitrile solutions of **1** results in the loss of reversibility of the reduction wave and the formation of daughter products marked by the appearance of an anodic wave at −0.25 V. Reduction of a CO-saturated acetonitrile solution of **1** on the time scale of preparative electrolysis (30 min) is accompanied by a change in the color of the solution from orange-red to green and the passage of ∼1.9 electrons/complex, consistent with its assignment to an overall two-electron process. The IR spectrum of the reduction product **1B** is relatively simple and matches closely to that obtained in thin-layer spectroelectrochemical experiments of **1** conducted under elevated pressures of CO described in the following section. Treatment of the catholyte, mainly containing **1B**, with 2 equiv of *p*-toluenesulfonic acid (HOTs) results in the partial recovery of **1** (∼40%; IR, Supporting Information) together with formation of dihydrogen (detected by gas chromatography) in yields of 20−40% based on the parent complex.

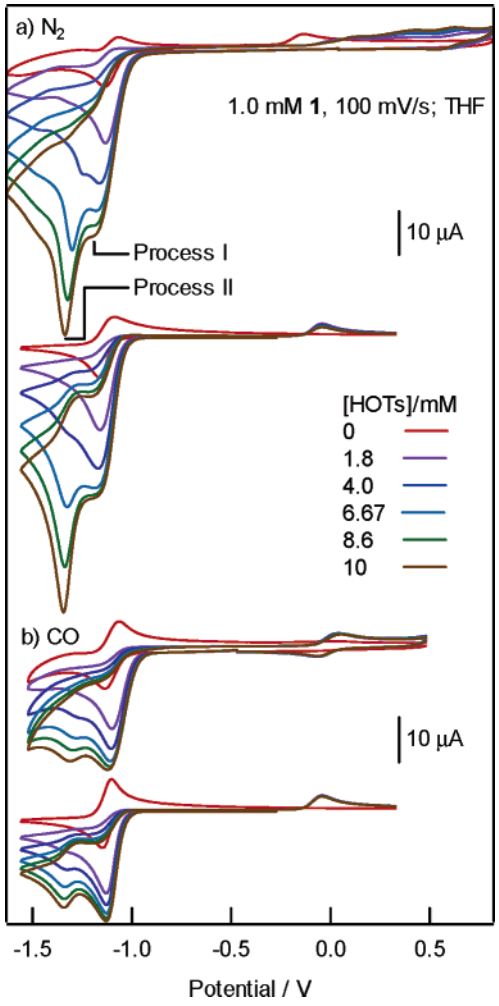

Figure 1. Cyclic voltammograms of **1** (1 mM) in 0−10 mM HOTs (2 mm diameter vitreous carbon working electrode, ν = 100 mV/s, 0.3 M TBA[ClO_4]/THF). The voltammograms are corrected for the effects of solution resistance. Solutions were saturated with either N_2 (a) or CO (b). Simulations of the voltammetry using Scheme 1 are given below the experimental data. Apart from the rate of dimerization of $\mathbf{1}^-$, identical values of the equilibrium and rate constants were used for both sets of simulations.

Electrocatalytic Proton Reduction. In the presence of the moderately strong acid HOTs (pK_a = 8 in CH_3CN),[22] the reduction of **1** is electrocatalytic with respect to proton reduction, and this is reflected both by the voltammetry (Figure 1) and by the identification of dihydrogen as a reduction product. The leading edge of the reduction wave of **1** shifts to more positive

(15) (a) Li, H.; Rauchfuss, T. B. *J. Am. Chem. Soc.* **2002**, *124*, 726−727. (b) Lawrence, J. D.; Li, H.; Rauchfuss, T. B. *Chem. Commun.* **2001**, 1482−1483. (c) Lawrence, J. D.; Li, H.; Rauchfuss, T. B.; Bénard, M.; Rohmer, M.-M. *Angew Chem., Int. Ed.* **2001**, *40*, 1768−1771.
(16) Zhao, X.; Georgakaki, I. P.; Miller, M. L.; Mejia-Rodriguez, R.; Chiang, C.-Y.; Darensbourg, M. Y. *Inorg. Chem.* **2002**, *41*, 3917−3928.
(17) Cheah, M. H.; Borg, S. J.; Bondin, M. I.; Best, S. P. *Inorg. Chem.* **2004**, *43*, 5635−5644.
(18) Shyu, S. G.; Wojcicki, A. *Organometallics* **1985**, *4*, 1457−1459.
(19) Zhou, T.; Mo, Y.; Liu, A.; Zhou, Z.; Tsai, K. R. *Inorg. Chem.* **2004**, *43*, 923−930.
(20) Mathieu, R.; Poilblanc, R.; Lemoine, P.; Gross, M. *J. Organomet. Chem.* **1979**, *165*, 243−252.
(21) Darchen, A.; Mousser, H.; Patin, H. *Chem. Commun.* **1988**, 968−970.
(22) Izutsu, K. *Acid−Base Dissociation Constants in Dipolar Aprotic Solvents*; Blackwell Scientific Publications: Oxford, 1990.

Scheme 1. Reaction Scheme Used for Digital Simulations of Electrocatalytic Proton Reduction in the Presence of **1** (Figure 1)[a]

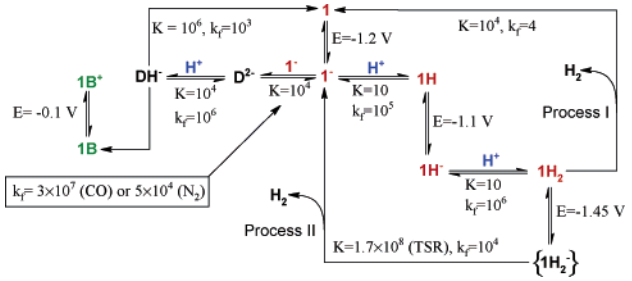

[a] In all cases, the rate constants for heterogeneous electron transfer and the diffusion coefficients were set at 1 cm s^{-1} and 10^{-5} cm^2 s^{-1}, respectively. The values of the equilibrium constants (K) and forward rate constants (k_f) are those used for the simulations in Figure 1 (TSR = thermodynamically superfluous reaction).

potentials, and at faster scan speeds and/or higher HOTs concentrations, two electrocatalytic waves are evident, one associated with the reduction of **1** ($E_{pc} \approx -1.12$ V, process I) and a second ($E_{pc} \approx -1.34$ V, process II) which does not have a counterpart in the voltammetry of **1** in the absence of protons (Figure 1). Whereas the reduction process is more reversible in the presence of additional CO, the peak catalytic current is lowered for solutions saturated with CO. Either additional CO impedes formation of the catalytically active species or CO reacts with the catalyst to effectively remove it from the cycle.

The changes in the voltammetry of **1** with a variation of proton concentration may be understood in terms of Scheme 1, as is shown by the digital simulations (Digisim[23]) in Figure 1. The one-electron reduction product, $\mathbf{1}^-$, reacts rapidly with protons, and this accounts for the shift of the reduction wave to more positive potentials. Since the addition of water (a weak acid) converts the reduction from a one- to a two-electron process, the reduction of **1H** occurs at potentials similar, or more positive, to that of **1**. Hydrogen evolution following protonation of $\mathbf{1H}^-$ would lead to recovery of **1** (process I). A reduction wave occurring at potentials similar to those of process II has previously been attributed to proton reduction at the vitreous carbon electrode (−1.4 V).[12] Under the conditions of these experiments, background proton reduction in the absence of **1** is slow and gives a broad current response <10% of that obtained at E_{pc} in the presence of **1** (1 mM). Moreover, the observation that the current associated with both process I and process II is lowered when the catalytic species is more rapidly lost from the solution (Figure 1b) is consistent with process II being attributed to an electrocatalytic reaction involving a species derived from **1**. This step may be assigned to either the reduction of $\mathbf{1H_2}$ or $\mathbf{1H}^-$. The latter alternative is unlikely since the reduction potentials of **1H** and $\mathbf{1H}^-$ are not easily reconciled if process II involves reduction of $\mathbf{1H}^-$. Moreover, reduction of $\mathbf{1H}^-$ is not observed at the required potentials in experiments conducted with acids of intermediate strength (CH_3COOH). Reduction of $\mathbf{1H_2}$ is arbitrarily assigned to a one-electron process, and elimination of dihydrogen from $\mathbf{1H_2}^-$ would lead to formation of $\mathbf{1}^-$ and account for the electrocatalytic wave designated process II. Scheme 1 is completed by inclusion of a reaction channel that accounts for the loss of the catalytic species. We have chosen to model this by a single pathway, and the series of steps involving dimerization of $\mathbf{1}^-$, followed by protonation and fragmentation, provides a close match of the details of the voltammetry under N_2 and CO. While the CO concentration is not explicitly included in this path, the different values for the forward rate constant of the first step in this reaction sequence are intended to reflect the effect of CO on the relative importance of this path. Whereas rearrangement of $\mathbf{1H}^-$ to **1B** would provide a simpler route to the loss of catalyst, simulations based on a pathway that is first order in $\mathbf{1}^-$ and protons neither give as close agreement between the form of the calculated and observed voltammograms nor reflect the insensitivity of E_{pc} for process II to the rate of loss of catalyst.

Simulations of the electrochemistry based on Scheme 1 involve four redox couples, seven homogeneous reactions, and a total of 13 chemical species. Since the numerical values of the equilibrium and rate constants are not of primary concern, the values of the diffusion coefficients and k_f (het) for the redox processes have been set to 1×10^{-5} cm^2 s^{-1} and 1 cm s^{-1}, and the k_f values for the protonation reactions have been set near 1×10^6. Notwithstanding the large number of variables remaining, the acid concentration dependence of the voltammetry constitutes a complex data set that can be used to assess the validity of the mechanism. It is noted that an alternate reaction scheme has recently been proposed for $Fe_2(\mu\text{-}SEt)_2(CO)_6$ in which a weak electrocatalytic wave at potentials similar to that of process II is attributed to a net two-electron reduction.[11] In light of this report, the possibility that process I involves a net one-electron reduction of **1** needs to be considered. While a mechanism based on this proposition may give a satisfactory model of the electrochemistry for higher concentrations of **1**, such a scheme requires a bimolecular step and is unable to account for the observed electrochemical response with changes to the concentration of **1**.

Spectroelectrochemical (SEC) Investigation of the Reduction of 1. Under elevated CO pressures (~0.2 MPa; 1 MPa ≈ 10 atm), electrochemical reduction of **1** results in near quantitative production of a single product, **1B**. When monitored using faster time scale SEC techniques, the reduction reaction can be seen to proceed with the initial formation and decay of an intermediate species, **1A** (Figure 2a). The reasonably well-defined spectral changes obtained during reduction of **1** suggest that **1A** cleanly converts to **1B**. The final spectrum obtained following reduction appears to have no contribution from **1A**, and the differences in the IR spectra of **1** and **1B** suggest that significant structural change accompanies reduction, consistent with the observation that only a small quantity of **1** is recovered by reoxidation at −400 mV (Supporting Information). The application of more strongly oxidizing potentials (+600 mV) results in the recovery of ~80% of **1** (Figure 2d) together with broad ill-defined residual ν(CO) bands attributed to iron-containing decomposition products.

Since **1A** and **1B** are the only products evident in the early stages of reduction of CO-saturated solutions of **1** and reoxidation of these solutions at −0.4 V gives a simple mixture of **1** and **1B**, the IR spectrum of **1** can be used to extract the spectra of **1A** and **1B**. A critical first step in the analysis of the chemistry is the identification of the redox states of the reduction products **1A** and **1B**. Since **1B** is moderately stable, conventional[24] and

(23) Rudolph, M.; Reddy, D. P.; Feldberg, S. W. *Anal. Chem.* **1994**, *66*, 589A−600A.

(24) Bard, A. J.; Faulkner, L. R. *Electrochemical Methods: Fundamentals and Applications*; John Wiley & Sons: New York, 1980.

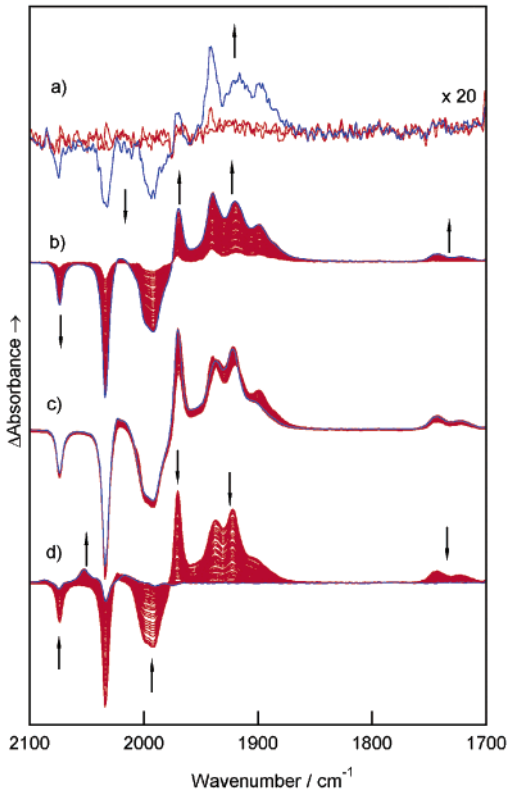

Figure 2. IR spectra recorded during the reduction (a−c) and reoxidation (d) of a 10 mM solution of **1** in THF (0.3 M TBA[ClO_4]) in the SEC cell under 0.3 MPa of CO. The Δ absorbance spectra were calculated using as reference a spectrum recorded immediately before the application of a reducing potential (time between spectra = 1.4 s, 3 mm vitreous carbon working electrode, ~25 μm layer of solution).

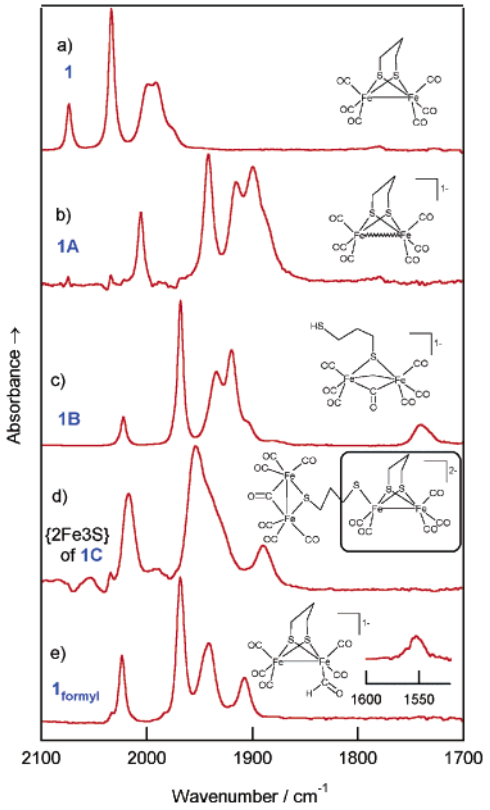

Figure 3. IR spectra in the ν(CO) region of **1** and the electrochemically or chemically reduced products thereof.

thin-layer[25] coulometric techniques can be employed, and these show that two electrons are required for the conversion of **1** into **1B**. The assignment of the redox state of the transiently stable species **1A** presents greater difficulties. Whereas the voltammetric response obtained for reduction of **1** suggests a one-electron process, it is not necessary that this product correspond to **1A**. In the thin-layer SEC experiments, it is possible to correlate the time evolution of the products with the coulometry, and the results of those experiments lend support to the proposition that the formations of **1A** from **1** and **1B** from **1A** both involve one-electron reduction.

Characterization of the One-Electron-Reduced Product, 1A. Confirmation of the assignment of **1A** to a redox state intermediate between **1** and **1B** would follow from the observation of disproportionation or comproportionation-type reactions. Thus, the decay of **1A** under open-circuit conditions is expected to be accompanied by an increase in the concentrations of both **1** and **1B**. A significant transient concentration of **1A** can be generated in thin-layer SEC experiments in the early stages of the reduction of carefully dried CO-saturated solutions of **1** in acetonitrile. If during this period the potentiostat is switched to an open circuit, the time evolution of the products can be monitored using IR spectroscopy. The results of such an experiment are shown in Figure 4. After the cell is switched to an open circuit (time = 0), the rapid depletion of **1A** is accompanied by an increase in the concentrations of *both* **1** and **1B**. Moreover, the lifetime of **1A** is longer for lower initial concentrations of **1**, suggesting that loss of **1A** occurs by a bimolecular reaction. Since the recovery of **1** is central to the assignment of the oxidation state of **1A**, it is important to ensure that the recovery of the starting material includes a component due to chemical reaction. Owing to concentration gradients developed during the experiment, recovery of **1** will include a component due to diffusion of **1** into the thin layer, and this is expected to have a linear $t^{1/2}$ dependence.[24] At short times (<10 s), diffusion clearly makes a minor contribution to the overall change in concentrations (inset of Figure 4). Therefore, the rapid increase in concentration of **1** is due to chemical reaction, and consequently, **1A** is in a redox state intermediate between **1** and **1B**.

The ν(CO) bands of metal carbonyls are sensitive to the charge state and geometry of the complex,[26] and the ν(CO) bands of **1A** have a similar profile to those of **1**, although shifted by ~70 cm^{-1} to a lower wavenumber. The magnitude of the shift of the ν(CO) bands is in keeping with a one-electron reduction delocalized over the two iron centers.[27] The conversion of **1A** to **1B** is accompanied by a smaller (~20 cm^{-1}) shift of the ν(CO) bands *to a higher wavenumber*, suggesting that **1A** and **1B** share common charge and/or oxidation states. If addition of the second electron is accompanied by either protonation or

(25) (a) Fleischmann, M.; Pletcher, D.; Rafinski, A. *J. Electroanal. Chem.* **1972**, *38*, 329−336. (b) Hinman, A. S.; Pons, S.; Cassidy, J. *Electrochim. Acta* **1985**, *30*, 95−99. (c) Salbeck, J. *J. Electroanal. Chem.* **1992**, *340*, 169−195.

(26) Nakamoto, K. *Infrared and Raman Spectra of Inorganic and Coordination Compounds, Part B: Applications in Coordination, Organometallic, and Bioinorganic Chemistry*, 5th ed.; John Wiley & Sons: New York, 1997; pp 126−148.

(27) (a) Hsu, H.-F.; Koch, S. A.; Popescu, C. V.; Münck, E. *J. Am. Chem. Soc.* **1997**, *119*, 8371−8372. (b) Jiang, J.; Acunzo, A.; Koch, S. A. *J. Am. Chem. Soc.* **2001**, *123*, 12109−12110.

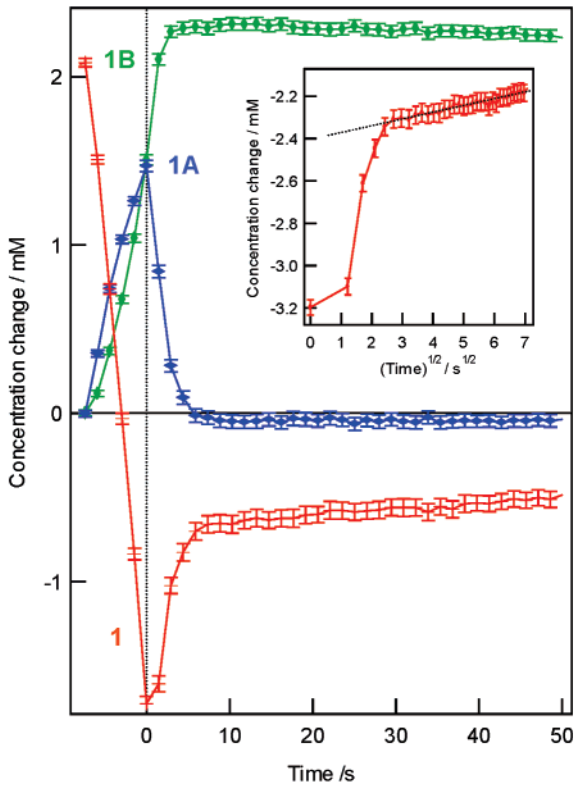

Figure 4. Time evolution of **1**, **1A**, and **1B** following the reduction of **1** (10 mM) for 7.5 s (−1.6 V, CH_3CN, 0.2 M TBA[ClO_4], $p(CO) = 0.3$ MPa) then switching the cell to an open circuit. An offset of 2.1 mM has been added to the concentration change of **1**. Concentrations were obtained by multicomponent analysis of the IR spectra with error bars drawn at the 3 esd confidence level. The inset shows the $(time)^{1/2}$ dependence of the concentration of **1**.

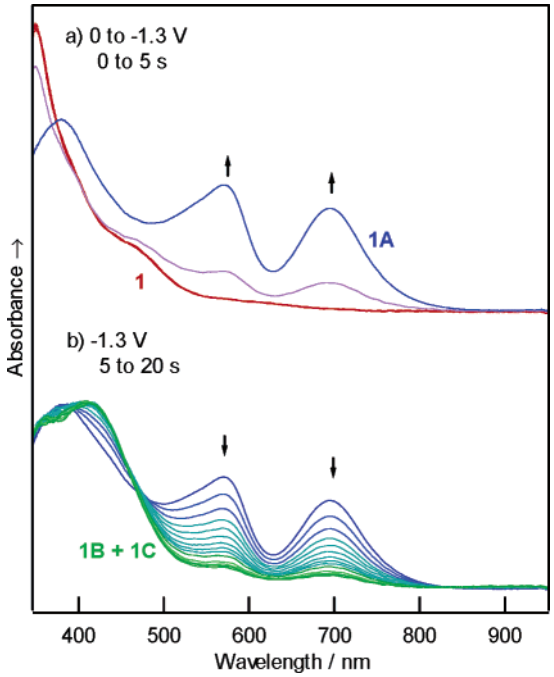

Figure 5. UV−vis spectra recorded during the reduction and reoxidation of **1** in DMF in the SEC cell under 0.7 MPa of CO. The species associated with each set of spectra are based on the analysis of the time and potential dependence of the IR spectra.

dissociation of an anionic ligand from the diiron center, **1A** and **1B** would share a common charge state.

The open-shell electronic structure proposed for **1A** should be reflected by distinctive UV−vis and EPR spectra. UV−vis SEC spectra recorded during the reduction of **1** reveal intense absorption bands at 580 and 700 nm, which may be attributed to **1A** (Figure 5). The conversion of **1A** into **1B** (with small amounts of **1C**) is associated with the decay of the longer wavelength bands and the appearance of a band at ∼420 nm. These spectral changes may be easily understood in terms of the reported Fenske−Hall calculations of $Fe_2(\mu\text{-SMe})_2(CO)_6$, which indicate that the frontier orbitals are predominantly metal based, being Fe−Fe bonding and antibonding in character.[28] The calculated HOMO−LUMO separation of ∼5−6 eV is consistent with the energy of the absorption bands [335 (s) and 460 (sh, w) nm] of **1**. The phosphido-bridged analogues of **1**, $[Fe_2(\mu\text{-PH}_2)_2(CO)_6]^{n-}$ (n = 0−2), are calculated to have similarly large HOMO−LUMO separations for the neutral and dianion complexes, whereas a much smaller HOMO−SOMO separation is calculated for the anion.[28,29]

Solutions containing steady-state concentrations of **1A** can be generated by reduction of carefully dried CO-saturated solutions of **1** during continuous-flow electrosynthesis experiments. If the solution flow is interrupted, the concentration of **1A** decays in a manner analogous to that observed in the thin-layer SEC experiments (Figure 4). The lifetime of **1A** is greatest at lowest solute concentrations, consistent with the decay of **1A** through a second-order reaction. Solutions containing significant concentrations of **1A** generated in this fashion, when rapidly frozen at 80 K, give a strong EPR signal with $g = 2.00$ (120 K, Supporting Information). The EPR signal is almost extinguished when these solutions are warmed to room temperature and quickly refrozen. Solutions of **1B** are EPR silent. Both the chemical and spectroscopic evidence strongly support the assignment of **1A** to species $\mathbf{1}^-$.

Formulation of the CO-Bridged Two-Electron-Reduced Product, 1B. The IR spectrum of **1B** has a profile closely related to that of a phosphido-bridged diiron compound previously formulated with a bridging CO group and a terminal hydride ligand, $[Fe_2(\mu\text{-PPh}_2)_2(\mu\text{-CO})H(CO)_5]^-$, $\mathbf{P_C}$.[30] More recently, this product has been reformulated as $[Fe_2(\mu\text{-PPh}_2)(\mu\text{-CO})(CO)_6]^-$, $\mathbf{P_R}$.[17] The more recent formulation would appear to be at odds with the observed hydridic chemistry of both **1B** and $\mathbf{P_C}$ where reactions with CCl_4, PhCOCl, and H^+ yield $CHCl_3$, PhCHO, and H_2, respectively, together with the respective parent compound. The structure and reactions of the 7-CO sulfur analogue of $\mathbf{P_R}$, $[NHEt_3][Fe_2(\mu\text{-2,4,6-}(CH_3)_3C_6H_2S)(\mu\text{-CO})(CO)_6]$, $[NHEt_3]\mathbf{S_R}$, have been reported by Seyferth and coworkers.[31] The IR spectrum reported for $\mathbf{S_R}$ is more complex than that obtained from **1B**; moreover, unlike **1B**, $\mathbf{S_R}$ is reported to be unreactive with benzoyl chloride even in refluxing THF.[31] In view of these differences in the chemistry and spectroscopy, an assignment of the structure of **1B** to one analogous to that of $\mathbf{S_R}$ requires strong supporting evidence.

(28) Hall, M. B.; Fenske, R. F.; Dahl, L. F. *Inorg. Chem.* **1975**, *14*, 3103−3117.
(29) Baik, M.-H.; Ziegler, T.; Schauer, C. K. *J. Am. Chem. Soc.* **2000**, *122*, 9143−9154.
(30) Collman, J. P.; Rothrock, R. K.; Finke, R. G.; Moore, E. J.; Rose-Munch, F. *Inorg. Chem.* **1982**, *21*, 146−156.
(31) Seyferth, D.; Womack, G. B.; Archer, C. M.; Dewan, J. C. *Organometallics* **1989**, *8*, 430−442.

The incorporation of a bridging CO group in the structure of **1B** is suggested by the appearance of a band at 1741 cm^{-1} (Figure 3c) and, on the basis of ^{13}CO isotopic substitution, is assigned to a CO vibration. The wavenumbers of bridging ν(CO) bands are known to be highly sensitive to solvent polarity and ion pairing.[31] Solutions of **1B** contain an equilibrium mixture of ion-paired and non-ion-paired forms; this is most evident with highly polarizing cations, such as Li^+, where in THF, the bridging ν(CO) band shifts from 1741 to 1670 cm^{-1}. At high concentrations, weakly ion-pairing ions, such as $[NBu_4]^+$, can perturb the spectrum, and this is reflected by the appearance of two more closely spaced bridging modes for **1B** generated electrochemically in THF (Figure 2). The solvent and counterion dependence of the IR spectra of **1B** is given as Supporting Information.

The incorporation of a hydridic hydrogen atom in the formulation of **1B** is suggested by the evolution of dihydrogen following the addition of acid to electrochemical preparations of **1B**. This would also appear to be supported by ESI-MS of chemically generated samples of **1B** obtained at low to moderate cone voltages (10−30 V). The spectra are dominated by molecular ions with m/z = 415, 387, and 359 amu that have isotope patterns matching that expected for $[Fe_2(\mu\text{-pdt})H(CO)_{5,6,7}]^-$. Significantly, there was no evidence for dimers or nonprotonated anions, $[Fe_2(\mu\text{-pdt})(CO)_{5,6,7}]^{2-}$. The presence of an additional hydrogen atom is supported by H/D exchange. Reaction of a sample of **1B** with D_2O immediately prior to the collection of the mass spectrum results in a mixture of $[Fe_2(\mu\text{-pdt})H(CO)_{5,6,7}]^-$ and $[Fe_2(\mu\text{-pdt})D(CO)_{5,6,7}]^-$ (Supporting Information). In terms of the CO composition of **1B**, the relative abundance of $[Fe_2(\mu\text{-pdt})H(CO)_7]^-$ is greater at lower cone voltages. The relative abundance of this ion does not appear to change upon saturation of the solution with dinitrogen or CO, suggesting that **1B** does not increase its CO/Fe stoichiometry during the measurement. However, in view of the possibility of CO addition or loss in the solvent desorption phases of the measurement, the CO stoichiometry of **1B** is not considered to be determined unambiguously in these experiments.

The proposition that **1B** results from the addition of two electrons and one proton to **1** would suggest its formation by reaction with a hydride source (e.g., $Li[HBEt_3]$). Reactions of this sort, conducted in CO-saturated acetonitrile, yield spectroscopically clean (IR) solutions of **1B**, which are relatively stable in the absence of dioxygen. Solid samples of **1B** have been prepared by reduction of **1** using $NaBH_4$ in CO-saturated THF in the presence of an excess of 18-crown-6-ether. While these preparations have failed to yield crystalline samples, they provide a well-defined source of **1B** for spectroscopic investigations.

The appearance of a weak resonance with $\delta = -8.84$ in the ^1H NMR spectra of **1B** in THF is consistent with a terminal hydride; however, the relative intensity of this feature varies between samples, and its integration relative to the protons of the pdt bridge in all cases suggests a hydride/pdt stoichiometry <1:2. An alternate structure, compatible with the ESI-MS results, would involve protonation and displacement of one of the bridging sulfur atoms of the pdt bridge. While no clearly defined ^1H thiol resonances were identified, freshly prepared samples of **1B** give distinct ^1H resonances for each of the three methylene groups of the pdt bridge (δ = 1.98 m, 2.16 t, and 2.29 t), where decoupling experiments confirm their assignment to a single pdt unit (Figure 6). The inequivalence of the three methylene groups requires asymmetric binding of the pdt group to the diiron core.

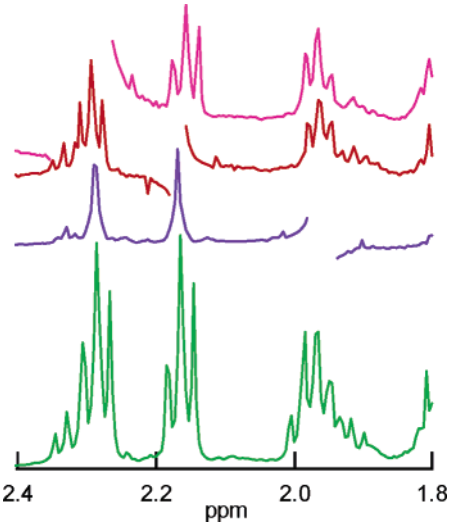

Figure 6. ^1H NMR spectra of a freshly prepared sample of [15-crown-5 Li]**1B** (d^8-THF) together with spectra obtained after proton decoupling at 1.96, 2.17, and 2.31 ppm.

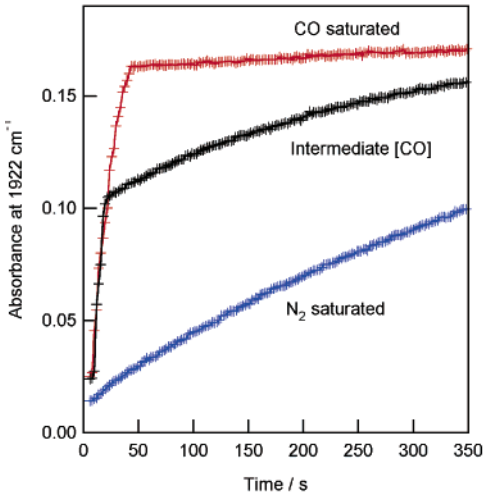

Figure 7. Rate of conversion of $\mathbf{1_{formyl}}$ into **1B** from solutions that are N_2-saturated, CO-saturated, or contain an intermediate concentration of CO.

The ESI-MS results provide qualified support for an increase in the CO/Fe ratio on conversion of **1** into **1B**, and this is confirmed by the [CO]-dependence of its formation, as described below. The initial product of reactions between **1** and $Li[HBEt_3]$, on the basis of its IR spectrum (Figure 3e), can be formulated as $[Fe_2(\mu\text{-pdt})(CHO)(CO)_5]^-$, $\mathbf{1_{formyl}}$. The IR spectrum of $\mathbf{1_{formyl}}$ is closely related to that obtained from a related formyl species formed by reaction between $Li[HBEt_3]$ and $Fe_2(\mu\text{-}PPh_2)_2(CO)_6$.[18] Well-defined solutions containing **1** and $\mathbf{1_{formyl}}$ may be formed in rapid-mixing experiments, and its decay into **1B** is followed by IR spectroscopy. The rate of conversion of $\mathbf{1_{formyl}}$ into **1B** is highly dependent on the concentration of free CO in solution, as shown in Figure 7. In the absence of free CO, the half-life of $\mathbf{1_{formyl}}$ is ~250 s, whereas in CO-saturated solutions, the reaction is complete within 30 s. Importantly, for solutions having an intermediate concentration of free CO, the reaction

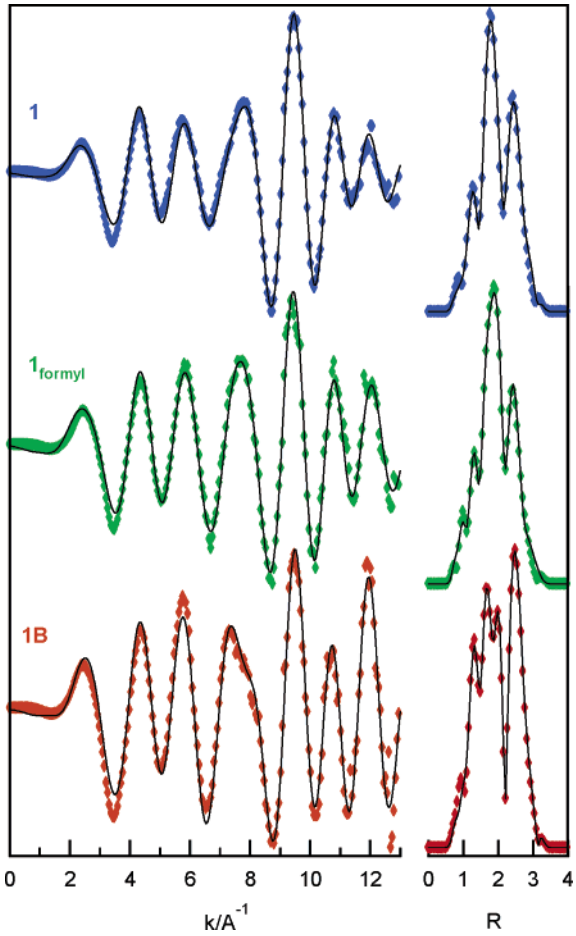

Figure 8. Iron *K* edge EXAFS and radial distribution functions of **1**, $\mathbf{1}_{\mathbf{formyl}}$, and **1B**.

proceeds in two steps with rates comparable to those obtained for CO- and N_2-saturated solutions. This observation requires that the concentration of free CO decrease as $\mathbf{1}_{\mathbf{formyl}}$ is converted into **1B** (i.e., that CO is consumed in the course of the reaction).

EXAFS Investigations. A remaining structural characteristic important to the deduction of the structure of **1B** is the nature of the metal−metal bonding interaction. In terms of electron counting, retention of the Fe−Fe bond of **1** following two-electron reduction and CO addition would require the formal loss of four electrons from the diiron core, and this may occur through dissociation of one of the sulfur atoms of the pdt ligand. Partial dissociation to give a pdt ligand with bridging and terminally bound S atoms would leave the methylene groups inequivalent (as required by the NMR results), but this would give a structure without a formal Fe−Fe bond. In the absence of a crystalline sample of the Fe−Fe, a good estimate of the distance may be obtained from the solute species by analysis of the X-ray absorption fine structure (EXAFS).[32] Solution iron *K* edge EXAFS spectra of **1**, $\mathbf{1}_{\mathbf{formyl}}$, and **1B** are shown in Figure 8. In broad terms, the similarity of the EXAFS and radial distribution functions of **1** and $\mathbf{1}_{\mathbf{formyl}}$ is readily understood in terms of a hydride attack at a ligand remote from the diiron core leaving the nearest neighbor Fe distances largely unaltered. As is evident from the IR spectra (Figure 3c), a more substantial change in the structure accompanies formation of **1B**, and the markedly different radial distribution function (Figure 8) indicates a significantly different coordination geometry of the iron atoms.

The information content of the EXAFS data may be expressed in terms of the number of independent points (N_{idp}); this has been defined by Stern in terms of the *k* and *R* range of the data used for analysis.[33] Within this definition, models with the number of refined parameters larger than N_{idp} give refinements that are considered to be overdetermined. For the current data, N_{idp} is in the range of 20−22, and in all models considered, the number of refined parameters has been restricted so as to give a ratio of N_{idp} to the number of refined parameters >1.5. The models used in the data analysis are summarized in Table 1. A satisfactory fit of the EXAFS data of **1** can be obtained using model **M1**, and this analysis yields structural parameters in close agreement with the crystal structure (Table 1). For $\mathbf{1}_{\mathbf{formyl}}$, the two iron atoms are inequivalent, and an ideal refinement would treat the two iron atoms as separate absorbers; however, this would increase the number of variables required in the model. Model **M2** is based on an average iron coordination environment where the increase in the number of refined parameters from 10 to 13 is needed to account for the formyl group identified through its absorption in the IR spectrum (Figure 3e). Since the formyl group makes a small relative contribution to the EXAFS, the Fe−C−O bond angle and C−O bond length were fixed at 120° and 1.18 Å, respectively, with the latter value being 0.02 Å longer than that of the terminal CO groups. Elimination of the formyl group from the model results in a significant deterioration in the refinement statistics; application of model **M1** to the formyl data resulted in an increase of the *R* value from 8.43 to 9.26%.

The IR spectrum of **1B** indicates the presence of a bridging CO group (Figure 3c), and model **M3** has this group aligned normal to the Fe−Fe bond and equidistant from the two iron atoms. The bridging CO bond distance is fixed at a value 0.02 Å longer than those of the terminal CO groups. In keeping with the increase in CO stoichiometry on conversion from $\mathbf{1}_{\mathbf{formyl}}$ to **1B**, three terminal CO groups are associated with each iron atom; the average coordination environment of which will comprise three terminal and one bridging CO group with the population of the bridging sulfur set at either one or two. Fits conducted using an average terminal CO population of $^5/_2$ gave similar refinement statistics. Although the refinement statistics for model **M3** are somewhat better when the S population is set to two, the fitting of the bridging CO group becomes problematic. Without restraints, the Fe−C_b distance refines to an unreasonably large value of 2.426 Å, and the Debye−Waller factor for the S atom of 5.86 is markedly larger than those found for the related compounds. While the corresponding fit with the S population set to one gives poorer *R* and χ^2 values, the unrestrained refinement of the bridging CO group gives a satisfactory Fe−C_b distance, although there is a substantial increase in the Debye−Waller values. Unlike the sulfur atom, which is more rigidly bound to the diiron core, the bridging CO group may take a range of conformations depending on whether there is ion pairing to the lithium cation, and this may reasonably account for the large Debye−Waller factor. It would appear that there is no significant statistical distinction between

(32) Zhang, H. H.; Hedman, B.; Hodgson, K. O. In *Inorganic Electronic Structure and Spectroscopy*; Solomon, E. I., Lever, A. B. P., Eds.; Wiley: New York, 1999; Vol. 1, pp 513−554.

(33) Stern, E. A. *Phys. Rev. B: Condens. Matter* **1993**, *48*, 9825−9827.

Table 1. Summary of the Refinements of the Solution EXAFS Data for **1**, $\mathbf{1_{formyl}}$, and **1B**

data	**1**	1_{formyl}	**1B**	
model[a]	**M1**	**M2**	**M3** (n=2)	**M3** (n=1)
		Distances[b] (Å)		
Fe−Fe	2.485 [2.508][c]	2.504	2.529	2.527 [2.494][d]
Fe−S	2.241 [2.251]	2.258	2.270	2.253 [2.304]
Fe−C	1.786 [1.795]	1.781	1.774	1.772 [1.75−84]
C−O	1.157 [1.135]	1.160	1.162	1.162 [1.135−62]
$Fe-C_{f/b}$		1.790	2.426	2.086 [1.926]
$C-O_{f/b}$		1.180[e]	1.180[e]	1.180[e] [1.208]
		DW × 1000		
C	0.95	2.98 (46)	0.90 (4)	0.96 (4)
O	1.93	2.26 (21)	1.69 (13)	1.92 (13)
$C_{f/b}$		0.973 (6)	1.12 (3)	20.2 (7)
$O_{f/b}$		18.8 (28)	2.3 (47)	11.8 (35)
Fe	1.64	1.31 (25)	2.44 (19)	2.19 (15)
S	1.005	1.39 (25)	5.86 (38)	2.01 (33)
E_0	−10.8 (21)	−7.53 (17)	−8.81 (14)	-8.85 (14)
S_0^2	0.744 (94)	0.706 (12)	0.699 (10)	0.699 (10)
N-refined	10	13	13	13
R_{XAFS} (χ^2)[f]	8.39% (1.46)	8.43% (0.91)	7.28% (0.60)	8.80% (0.87)
k range	0.5−13.2	0.5−12.2	0.5−13.3	0.5−13.3

[a] **M1** **M2** **M3**

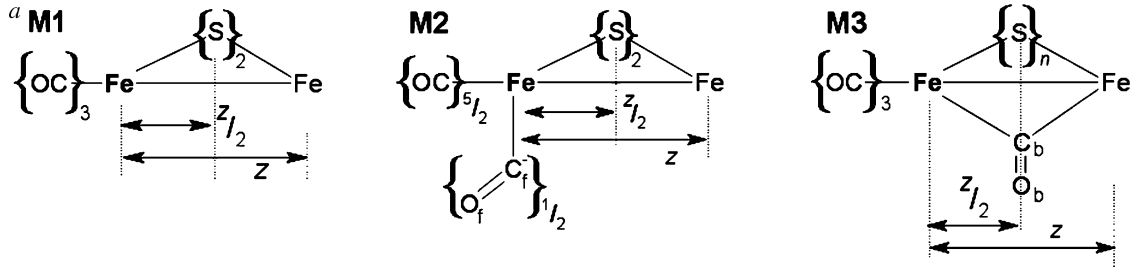

[b] Unless otherwise stated the error in the bond lengths is the typical systematic error of 0.02 Å. [c] X-ray data from ref. 34. [d] From X-ray structure of $[NHEt_3]\mathbf{S_R}$ ref 31. [e] C−O distance constrained to be 0.02 Å longer than the terminal C−O distance. [f] $\chi^2 = \int_{k=0...\infty}[w(\chi_{obs}(k)-\chi_{calc}(k))]^2$, $R_{XAFS} = \int_{k=0...\infty}[\chi^2/\chi^2_{calc\equiv O}]^{1/2}$; $\chi_{obs}(k)$ and $\chi_{calc}(k)$ are the observed and calculated EXAFS and w is a weighting factor.[35]

fits conducted using one or two sulfur atoms, and this appears to be due to correlations involving the parameters of the bridging CO group.

While the analysis of the EXAFS data reveals the general features of the structures, the differences in refinement statistics of themselves, do not give a clear distinction between the alternate structures for **1B**. Whereas the internuclear separations will generally be sensitive to the model, the estimate of the Fe−Fe distance is relatively model independent owing to the difference in atomic number of the iron atom and the other backscatters. The Fe−Fe separation of 2.527 Å is in a range compatible with the presence of an Fe−Fe bond, with this being slightly longer than the value of 2.494 Å obtained for $\mathbf{S_R}$ where the bridging thiolate ligand is 2,4,6-$(CH_3)_3C_6H_2S^-$.[31] The diphenylphosphido-bridged analogue of $\mathbf{S_R}$ has an Fe−Fe distance of 2.601 Å. Therefore, the short Fe−Fe distance, when taken together with the redox state and CO stoichiometry, strongly supports the structure for **1B** shown below.

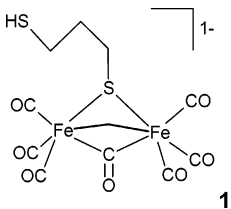

1B

Mössbauer spectra obtained from frozen acetonitrile solutions of **1B** (80 K) are dominated by a single doublet having an isomer shift of 0.001(3) mm s^{-1} with a rather large quadrupole splitting (QS) of 1.684(7) mm s^{-1} (Supporting Information), which implies a highly asymmetrical electron distribution about the diiron core. A large value of the QS (1.53 mm s^{-1}) is also observed for $[Fe_2(\mu\text{-}PMe_2)_2(CO)_6]^{2-}$.[36] Whereas the half-widths of the resonances of **1B** are relatively large [0.157(6) mm s^{-1}], the observation of a single doublet implies that the environment about the two iron atoms is similar. Clearly, the proposed structure for **1B** satisfies this requirement.

Intermediates Formed during Electrocatalytic Proton Reduction. The current and spectral response obtained during the reduction of **1** in a thin-layer SEC experiment is shown in Figure 9a. With the application of a reducing current (time = t_0), there is rapid depletion of the starting material within the thin layer, and this may be monitored by the depletion of the 2032 cm^{-1} band of **1**. Exhaustive electrolysis of the 25 μm layer requires ∼40 s and is complete at t_1. At longer times, the composition of the solution trapped between the working electrode and the CaF_2 window reaches a steady state, as is evident by the absence of spectral change; the lower rate of charge flow reflects the rate of diffusion of fresh solution into the thin layer. The charge transferred between t_0 and t_1 will be related to the volume of solution in the thin layer, the solute concentration, and the number of electrons involved in the redox process. As expected from the analysis of the electrochemistry, the formation of **1B** requires the passage of ∼2 F mol^{-1} of **1**.

(34) Lyon, E. J.; Georgakaki, I. P.; Reibenspies, J. H.; Darensbourg, M. Y. *Angew. Chem., Int. Ed.* **1999**, *38*, 3178−3180.
(35) Ellis, P. J.; Freeman, H. C. *J. Synchrotron Radiat.* **1995**, *2*, 190−195.
(36) Dessy, R. E.; Rheingold, A. L.; Howard, G. D. *J. Am. Chem. Soc.* **1972**, *94*, 746−752.

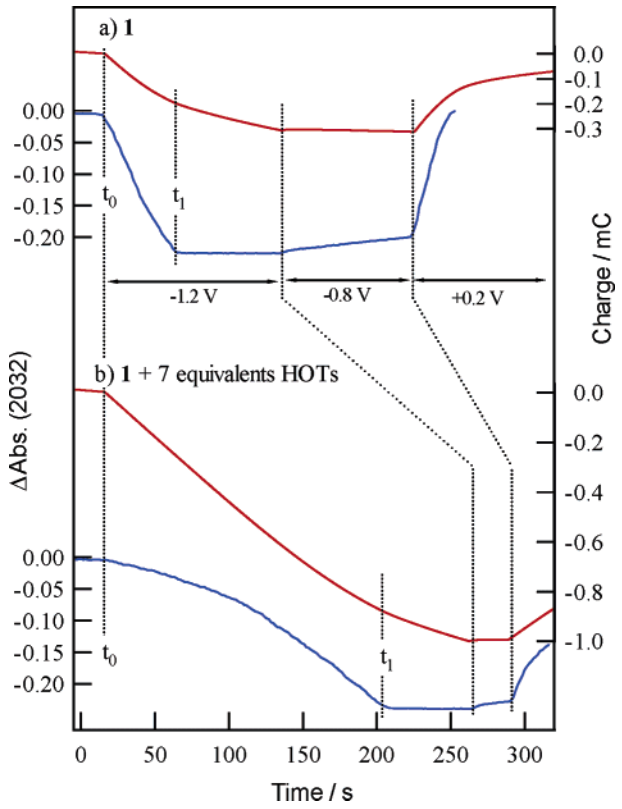

Figure 9. Time evolution of the depletion of **1** (as given by Δ absorbance at 2032 cm^{-1}) and charge passed during thin-layer (25 μm) SEC experiments for solutions containing (a) **1** (10 mM, THF, 0.2 M TBA[ClO_4]) and (b) a solution as above + 7 equiv of HOTs.

The addition of acid to the solution results in a marked increase in the charge passed into the layer with a lower apparent rate of reduction of **1**. During the 190 s required for reduction of a mixture of **1** and 7 equiv of HOTs, ~10 F mol^{-1} of **1** is passed into the solution (Figure 9), in agreement with the expected value (9 F mol^{-1}). It is evident that a net reduction of **1** occurs only as the proton concentration is depleted within the thin layer (Figure 9b). Experiments conducted using different acid concentrations give a current response similarly related to the concentrations of **1** and HOTs, and analogous experiments conducted on acid solutions in the absence of **1** give a significantly smaller current response. These observations require that **1** be recovered during the electrocatalytic cycle and that formation of **1B** predominantly occurs in the final stage of the reaction. Both aspects of the chemistry are well modeled by Scheme 1.

During the latter stages of the reduction of **1**/HOTs, an additional species can be identified that features ν(CO) bands at 2062, 2016, 1985, 1964, and 1789 cm^{-1} (Figure 10), the wavenumbers of which are consistent with assignment to a neutral dithiolate-bridged diiron carbonyl compound having a bridging carbonyl group. If the potentiostat is switched to open circuit in the time interval when these bands are present in the spectra, they are found to decay at a slow rate, suggesting that in the absence of a reducing potential, this species is stable to further reaction. The two neutral compounds proposed in Scheme 1, **1H** and $\mathbf{1H_2}$, are candidates for assignment to this species. Since electrocatalysis associated with process I is attributed to dihydrogen elimination from $\mathbf{1H_2}$, the intermediate species is more likely to be attributed to **1H**. In this event, the

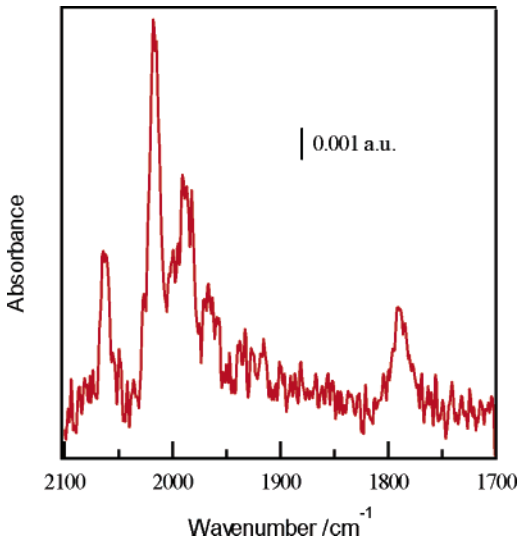

Figure 10. IR spectrum of the transiently stable species formed during electrocatalytic proton reduction in the presence of **1**.

Scheme 2. Proposed Reaction Path for Formation of **1B** and **1** from **1A**

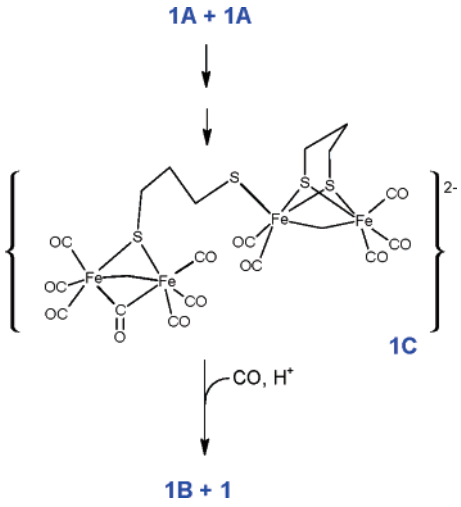

apparent stability of **1H** would contrast with that of the other one-electron-reduced product, $\mathbf{1}^-$ (Figure 4). The stabilization of the one-electron reduced product by protonation is understood in terms of the expected shift in its reduction potential to more positive values. In the presence of a reducing potential, this will lead to further reduction (Scheme 1), but in the absence of a reducing potential, the protonated species will be a less strong reducing agent.

Whereas $\mathbf{1}^-$ reacts to give **1** and **1B** in the absence of acids, protonation of $\mathbf{1}^-$ may permit trapping of the one-electron-reduced species. Thermodynamic considerations preclude the disproportionation of $\mathbf{1}^-$ to give **1** and **1B**, and this is consistent with the formulation of **1B**. Instead, it is proposed that electron and CO transfer occur through a CO-bridged intermediate that rearranges to give the pdt-bridged species, **1C**, shown in Scheme 2. Chemical and electrochemical reduction of **1** under an inert atmosphere leads to a series of products that are more complex than the corresponding reactions conducted under an atmosphere of CO (Supporting Information). After subtraction of the bands due to **1**, **1A** ($\mathbf{1}^-$), and **1B**, a set of ν(CO) bands attributed to **1C** remains in the spectrum (Figure 3d). Since the proposed

structure of **1C** consists of a **1B**-like fragment linked to a 2Fe3S fragment, the subtraction process will yield the ν(CO) bands of the 2Fe3S fragment of **1C**. The ν(CO) bands of this fragment have a profile closely matching that of $Fe_2((\mu\text{-}SCH_2)_2CHSR)(CO)_5$, **Fe2S3**,[37] although shifted by $\sim$30−40 cm^{-1} to a lower wavenumber. A shift of this magnitude may readily be explained in terms of the differing donor properties of the thioether and thiolate sulfur atoms. It is noted that the path for loss of the catalyst shown in Scheme 1 includes a step that is bimolecular in terms of $\mathbf{1}^-$. The more effective loss of catalyst under CO may be understood in terms of the final step of Scheme 2. The reversibility of the electrochemistry in the presence of CO, without protons, requires that protonation of the terminally bound sulfur atom of the pdt ligand is necessary for fragmentation of the dimer (into **1B** and **1**) to perturb the current response in cyclic voltammetric experiments.

Conclusion

The application of a range of electrochemical and SEC techniques has permitted the elucidation of the chemistry following reduction of **1**. Reduction proceeds in one-electron steps, with the lifetime of the initial product, $\mathbf{1}^-$, sufficient to permit spectroscopic (IR, UV−vis, and EPR) characterization. Whereas the addition of two electrons to the Fe−Fe bond would give an electron-precise product, there is no clear evidence for formation of such a species. These observations contrast with those from the phosphido-bridged diiron analogues where two-electron reduction leads to formation of a well-defined dianion having a planar 2Fe2P core.[17,38] Clearly, a planar 2Fe2S core is not possible for the pdt-bridged compounds, and this structural constraint may be responsible for the reduced relative stability of the dianion. While this proposition is superficially attractive, it has previously been reported that $Fe_2(\mu\text{-}SR)_2(CO)_6$ compounds also undergo separate one-electron reductions,[11] and our preliminary experiments suggest that the reductions of these compounds give products analogous to those obtained for **1**.

Whereas the ν(CO) bands of $\mathbf{1}^-$ and **1B** are similar in wavenumber, the latter is a two-electron-reduced product where charge is lost from the diiron core by dissociation of one of the sulfur atoms of the pdt group. Consistent with the assignment of the redox levels of the compounds, $^{13}CO/^{12}CO$ exchange only occurs at a significant rate when $\mathbf{1}^-$ is present in the solution; when presented with ^{13}CO, solutions of **1** and **1B** are similarly inert to CO exchange. It is well-known that 17- or 19-electron metal carbonyl complexes undergo rapid ligand exchange.[39] Reduction of **1** carried out using solutions saturated with either CO or N_2 results in the formation of a product (**1C**) that, on the basis of its IR spectrum, includes a diiron fragment in which one of the CO groups is replaced by a terminally bound thiolate ligand. This product is most likely dimeric where a pdt ligand bridges two diiron centers, with one sulfur bridging two iron atoms and the other bound terminally to one of the iron atoms of a second diiron fragment. This species may then rearrange to give **1B**.

The structure of **1B** has been considered in light of a range of spectroscopic and EXAFS results, and these suggest a 7-CO structure with a single sulfur atom of the pdt ligand bridging the diiron center. Whereas **1B** reacts with acid to recover **1**, the reaction is slow and **1B** is a kinetically unreactive side product in Scheme 1. The slow hydride transfer chemistry of **1B** must therefore be associated with an equilibrium involving rearrangement of the pendant thiol to give a hydridic species. Equilibria of this sort are the subject of further investigation and have been proposed for the diphenylphosphido-bridged analogue of **1B**.[17]

Electrocatalytic proton reduction by **1** is similarly rapid as the cyano/phosphine-substituted[12] complex and somewhat slower than the azadithiolate-bridged[14] analogues. The electrochemical response is comparatively well defined in THF and is amenable to digital simulation. Process I involves the elimination of dihydrogen following $2e^-/2H^+$ reaction of **1**, where a second process becomes important at higher acid concentrations. The differences in the voltammetry for acid solutions saturated with either N_2 or CO are best modeled in terms of the loss of catalyst by a reaction that is second order in terms of $\mathbf{1}^-$, and this is consistent with the formation of a dimer en route to formation of **1B** (Scheme 2). This species is formed more rapidly in the presence of excess CO, and under these conditions the electrocatalytic current is reduced. Paradoxically, the presence of additional CO leads both to more reversible electrochemistry of **1** and to poorer electrocatalysis. While poisoning of the catalyst by CO is a feature of the chemistry of both **1** and the H-cluster, the mechanism of inhibition of proton reduction is clearly different in the two cases.

The mode of hydride binding during electrocatalytic proton reduction would appear to be different for the phosphido- and thiolato-bridged diiron carbonyl compounds. Since reduction of the phosphido-bridged compounds leads to cleavage of the Fe−Fe bond, protonation must initially give terminally bound hydrides. There is strong evidence for the formation of $(\mu\text{-}PR_2)_2[FeH(CO)_3]_2$ following protonation of the corresponding dianion.[17,40] In this case, further reduction is needed to obtain dihydrogen evolution. On the other hand, it is well established that protonation of the electron-rich dithiolato-bridged diiron compounds gives bridged hydrides.[12,16,41] It would be expected that protonation of the one-electron-reduced products would follow a similar course. This proposition is not yet proven and may need re-evaluation in light of calculations examining the influence of electronic effects on the geometry of a series of complexes, $[L(CO)(CN)Fe_p(\mu\text{-}pdt)Fe_d(CO)_2(CN)]$.[42] From a starting point in which the two edge-shared square pyramidal units are aligned with the apical positions trans to the Fe−Fe bond, there are varying degrees of rotation of the $Fe_d(CO)_2(CN)$ group to give a bridging Fe_p−CO interaction according to the reduction level of the complex and the electron richness of the ligand, L, bound to Fe_p.[42] Basal/axial CO exchange[43] and CN^- substitution of CO for both **1** and **Fe2S3**[37,44] proceed through intermediates in which one of the CO groups is rotated

(37) Razavet, M.; Davies, S. C.; Hughes, D. L.; Barclay, J. E.; Evans, D. J.; Fairhurst, S. A.; Liu, X.; Pickett, C. J. *Dalton Trans.* **2003**, 586−595.
(38) Ginsburg, R. E.; Rothrock, R. K.; Finke, R. G.; Collman, J. P.; Dahl, L. F. *J. Am. Chem. Soc.* **1979**, *101*, 6550−6562.
(39) Cotton, F. A.; Wilkinson, G. *Advanced Inorganic Chemistry*, 5th ed.; Wiley-Interscience: New York, 1988; p 1305.
(40) Dobbie, R. C.; Whittaker, D. *Chem. Commun.* **1970**, 796−797.
(41) (a) Arabi, M. S.; Mathieu, R.; Poilblanc, R. *J. Organomet. Chem.* **1979**, *177*, 199−209. (b) Fauvel, K.; Mathieu, R.; Poilblanc, R. *Inorg. Chem.* **1976**, *15*, 976−978.
(42) Bruschi, M.; Fantucci, P.; De Gioia, L. *Inorg. Chem.* **2004**, *43*, 3733−3741.
(43) Lyon, E. J.; Georgakaki, I. P.; Reibenspies, J. H.; Darensbourg, M. Y. *J. Am. Chem. Soc.* **2001**, *123*, 3268−3278.
(44) George, S. J.; Cui, Z.; Razavet, M.; Pickett, C. J. *Chem.—Eur. J.* **2002**, *8*, 4037−4046.

into a bridging position. In the latter case, the rotation of the $Fe(CO)_3$ group, in such a way, opens a coordination site for the entering ligand. An intermediate with a similar geometry, but with a bridging hydride, has been proposed as the active species during photocatalytic H/D exchange of D_2/H_2O mixtures by $[Fe_2(\mu\text{-pdt})(\mu\text{-H})(CO)_4(PMe_3)_2]^+$.[16] In terms of the mechanism of electrocatylic proton reduction by **1** and its relationship to the H-cluster, the characterization of the $1e^-/1H^+$ product (**1H**) is of critical importance. While the transient appearance of a CO-bridged species during proton reduction is tantalizing, further work is needed in order to confirm its assignment to **1H**.

Experimental Section

General Procedures. Samples of $Fe_2(\mu\text{-pdt})(CO)_6$, **1**, were prepared by literature methods[43] and confirmed to be pure by spectroscopic and electrochemical analyses. Solvents were purified and dried by standard methods[45] and distilled under an atmosphere of dinitrogen immediately prior to use. Solutions used for electrochemical or spectroscopic analyses were prepared under an atmosphere of dinitrogen or argon using either standard Schlenk techniques or with the aid of a vacuum atmospheres glovebox. High purity Ar, N_2, and CO were obtained from BOC gases. The tetra-*n*-butylammonium perchlorate (TBA[ClO_4]) or tetra-*n*-butylammonium tetrafluoroborate (TBA[BF_4]), used as supporting electrolyte, was prepared and purified using standard procedures.[46]

CAUTION! Perchlorate salts are potentially explosive. Solutions containing TBA[ClO_4] as supporting electrolyte should not be allowed to evaporate to dryness.

Preparation of 1B. To a solution of **1** (143 mg, 0.37 mmol) in CO-saturated THF (10 mL) were added 18-crown-6 ether (98 mg, 0.37 mmol) and, finally, $NaBH_4$ (28 mg, 0.74 mmol). The reaction mixture was stirred at room temperature overnight to give a dark-green solution. The solvent was removed in a vacuum to give an olive-green oily residue which was washed with diethyl ether and then toluene three times. The washed residue was dried in vacuo to yield a greenish-yellow solid. Found: C, 36.27; H, 4.93; N < 0.3. Calcd for [18-crown-6-Na][$Fe_2(\mu\text{-}S(CH_2)_3SH)(CO)_7$] ($C_{22}H_{31}O_{13}S_2NaFe_2$): C, 37.63; H, 4.45. IR {ν(CO), THF}: 2022, 1968, 1935, 1920, and 1740 cm^{-1}.

A description of the preparation of the tetrabutylammonium and lithium salts, together with a tabulation of their IR active ν(CO) bands in a range of solvents, is given in the Supporting Information. When Li[$HBEt_3$] is used as the reducing agent, the reactions proceed much more rapidly. The corresponding reactions when completed on solutions saturated with dinitrogen give a complicated mixture of products that include **1B**.

Exhaustive electrolysis of **1** (88 mg, 0.023 mmol) at −1.5 V (vs Ag/AgCl) in 3 mL of a CO-saturated acetonitrile/TBA[BF_4] (0.1 M) solution with an excess of degassed water consumed 1.9 ± 0.2 F mol^{-1} of **1** (mean of five experiments). The olive-green catholyte gave an IR spectrum identical to that of **1B** prepared chemically. The electrochemical preparation of **1B** was performed in a gastight H-type electrochemical cell at both room temperature and ice-cold temperature using a vitreous carbon working electrode. The addition of 4 equiv of HOTs to the catholyte resulted in the evolution of dihydrogen. The yield of dihydrogen evolution ranged from 20 to 40%, based on **1B**, and this was measured by gas chromatography. The IR spectrum of the reaction mixture indicated partial recovery of **1** (20−40%), with there being no other metal carbonyl product.

Electrochemistry and Spectroelectrochemistry (SEC). Cyclic voltammetry experiments were controlled using an Autolab PGSTAT30 potentiostat with GPES software and were carried out in a one-compartment glass cell using a 2 mm diameter vitreous carbon working, platinum counter, and jacketed silver wire reference electrodes. The potential of the reference electrode was determined using the ferrocenium/ferrocene (Fc^+/Fc) couple, and all potentials are quoted relative to the SCE reference electrode. Against this reference, the Fc^+/Fc couple occurs at +0.38 V in acetonitrile and +0.53 V in THF.[47] Voltammograms were corrected for the effects of *iR* drop using a positive feedback approach implemented within the GPES software. Digital simulation of the voltammograms was conducted using Digisim (Version 3.03, Bioanalytical Systems).[23] The uncompensated voltammograms and simulation model parameters are included in the Supporting Information.

A PAR model 362 scanning potentiostat was used for the SEC experiments, and these were conducted using a purpose-built reflection−absorption cell capable of operating at moderate gas pressures (1 MPa). The design and operation of the high-pressure SEC cell has previously been described.[48] The current response of the SEC cell was monitored using a Powerlab 4/20 interface and recorded with Chart 4 software (ADInstruments). The solution under spectroscopic interrogation comprised a 10−30 μm layer of solution trapped between the multielectrode and a CaF_2 window. The thickness of the layer was adjusted under micrometer control and its value estimated using the extinction coefficients of absorptions due to the solvent.[49]

The IR−SEC spectra were collected in single beam mode, and differential absorbance spectra were calculated from these using the spectrum recorded immediately prior to the application of the potential step as the reference. Spectra for the individual reduced species were obtained by spectral subtraction using Grams/32 AI software (Galactic). In cases where the band profiles of the component species were overlapping, their relative concentrations were obtained by multicomponent analysis using routines available within the Igor Pro program (Wavemetrics).

Continuous-flow electrosynthesis experiments were carried out using a purpose-built cell that incorporates a reticulated carbon working electrode. The design of the cell has previously been reported.[50]

Instrumentation. Infrared spectra were collected using a Biorad FT175C FTIR spectrometer utilizing a Ge/KBr beam splitter and a narrow-band MCT detector. A Bruker ECS 106 X-band spectrometer was used to collect EPR spectra, and a Varian Unity Plus 400 MHz instrument was used to record NMR spectra.

UV−vis spectra were collected using an Instaspec II PDA detector coupled to a MS125 spectrograph (Oriel Instruments) that was fitted with a 300 g/mm grating. This combination permits the collection of spectra between 400 and 1050 nm in a single exposure. A 50 W tungsten lamp (Wotan HLX 64610) served as the source, and the optical path was constructed using off-axis parabolic mirrors (Melles Griot POA017).

Electrospray mass spectra were recorded using a Micromass Quattro II mass spectrometer in negative ion mode. Deoxygenated acetonitrile was used as the mobile phase and N_2 as the drying and nebulizing gas. Sample concentrations were approximately 0.4 μM.

Mössbauer spectra were recorded using an ES-Technology MS-105 spectrometer with a 200 MBq ^{57}Co source in a rhodium matrix at room temperature. Spectra were referenced to a 25 μm iron foil at 298 K. Parameters were obtained by fitting the data to Lorentzian band profiles.

Hydrogen evolution was quantified by gas chromatography measurements using a Shimadzu GC-14B equipped with a thermal conductivity detector (TCD). A standard containing 18×10^{-9} M H_2 in argon (at 0.1 MPa) was used for calibration.

(45) Errington, R. J. *Guide to Practical Inorganic and Organo-Metallic Chemistry*; Blackie Academic & Professional: London, 1997.
(46) Sawyer, D. T.; Sobkowiak, A.; Roberts, J. J. L. *Electrochemistry for Chemists*, 2nd ed.; Wiley-Interscience: New York, 1995; p 336.
(47) (a) Chang, D.; Malinski, T.; Ulman, A.; Kadish, K. M. *Inorg. Chem.* **1984**, *23*, 817−824. (b) Connelly, N. G.; Geiger, W. E. *Chem. Rev.* **1996**, *96*, 877−910.
(48) Borg, S. J.; Best, S. P. *J. Electroanal. Chem.* **2002**, *535*, 57−64.
(49) (a) Christensen, P. A.; Hamnett, A.; Higgins, S. J.; Timney, J. A. *J. Electroanal. Chem.* **1995**, *395*, 195−209. (b) Goplen, T. G.; Cameron, D. G.; Jones, R. N. *Appl. Spectrosc.* **1980**, *34*, 657−691.
(50) Bondin, M. I.; Foran, G.; Best, S. P. *Aust. J. Chem.* **2001**, *54*, 705−709.

EXAFS. X-ray fluorescence measurements were made at a temperature of ~10 K using beamline 20B (bending magnet) at the KEK Photon Factory (Tskuba, Japan). A channel-cut Si(111) monochromator provided an energy resolution ($\Delta E/E$) of $\sim 2.4 \times 10^{-4}$, and higher-order harmonics of the selected wavelength were rejected by detuning the monochromator by a factor of $^1/_2$. EXAFS measurements were conducted at the Fe *K* edge (7111.2 eV). Solutions were measured in fluorescence mode using a 10-element Ge detector and were prepared so as to give a concentration of 3−5 mM (i.e., 6−10 mM in iron) in THF.

Samples of $\mathbf{1_{formyl}}$ were generated by reaction with $Li[HBEt_3]$ in a continuous-flow experiment in which the product solution could be monitored in line by IR spectroscopy prior to collection in the EXAFS fluorescence cell. A Shimadzu Prestige FTIR was available at the beamline for spectroscopic characterization of the sample. Once a suitable sample was obtained, the solution was rapidly frozen and stored at 80 K prior to transfer to the 10 K cryostat. Samples of **1B** were prepared by either chemical reaction in THF (as described for $\mathbf{1_{formyl}}$) or electrochemically in CH_3CN using a continuous-flow electrosynthesis cell.[17] EXAFS spectra were indistinguishable for samples prepared by either method.

Data reduction of experimental X-ray absorption spectra was performed using the program XFIT[35,51] using a protocol that has recently been described.[17] The model structures were refined using the XFIT[35,51] software package, which incorporates ab initio FEFF 6.01[52] MS curved-wave calculations. The calculations included MS paths with $R_{max} = 3.5$ Å and up to four legs. The plane wave and curved wave path filter thresholds were set at 2 and 3% of the strongest MS path, respectively. A nonlinear least-squares fitting was used to vary the model and concurrently optimize the fit of the calculated to the observed EXAFS.[35] The goodness of fit parameter (R_{XAFS}) has been defined where an R_{XAFS} value around 20% is considered a good fit to the non-Fourier transformed data, while an R_{XAFS} value >40%, is poor.[51] The random (statistical) errors (σ_r) in the Fe−L bond lengths due to noise in the EXAFS data were estimated by Monte Carlo calculations.[35,51] In all cases, the values of σ_r were much less than the typical systematic errors (σ_s) and were assigned a conservative consensus value of 0.02 Å.[51] Details of the symmetry constraints and restraints on E_0, S_0^2, and σ^2 are available as Supporting Information.

(51) Gurman, S. J. *J. Synchrotron Radiat.* **1995**, *2*, 56−63.
(52) Zabinsky, S. I.; Rehr, J. J.; Ankudinov, A.; Albers, R. C.; Eller, M. J. *Phys. Rev. B: Condens. Matter* **1995**, *52*, 2995−3009.

Acknowledgment. We thank the Australian Research Council and BBSRC for funding this work, the ARC International Research Exchange Program (IREX) for providing travel funds to S.P.B., S.J.B., C.J.P., and M.R., the ARC for the award of an Australian Postgraduate Research Studentship to S.J.B., and the John Innes Foundation for the award of a studentship to M.R. The EXAFS experiments were performed at the Australian National Beamline Facility with support from the Australian Synchrotron Research Program, which is funded by the Commonwealth of Australia under the Major National Research Facilities Program. Mr. Mark I. Bondin (EPR and EXAFS), Dr. Garry Foran (EXAFS), Dr. David Evans (Mössbauer), and Professor Stephen Feldberg (Digisim) are thanked for technical assistance and/or advice.

Supporting Information Available: Electrochemistry and IR spectroelectrochemistry EPR of **1A**; ESI-MS and Mössbauer spectra of **1B**; IR spectra recorded during conversion of $\mathbf{1_{formyl}}$ to **1B**; parameters used for electrochemical simulations according to Scheme 1; description of chemical and electrochemical modes of preparation of **1B**; acid quenching of chemically and electrochemically generated **1B**; and constraints and restraints on EXAFS modeling of **1**, $\mathbf{1_{formyl}}$, and **1B**. This material is available free of charge via the Internet at http://pubs.acs.org.

JA045281F